J Solid State Electrochem (2012) 16:1893–1900
DOI 10.1007/s10008-011-1597-z

ORIGINAL PAPER

Resolution of the mechanism of CO electrooxidation on steady state and evaluation of the kinetic parameters for Pt and Ru electrodes

María S. Rau · María Rosa Gennero de Chialvo · Abel C. Chialvo

Received: 9 July 2011 / Revised: 7 November 2011 / Accepted: 10 November 2011 / Published online: 26 November 2011

Abstract The carbon monoxide oxidation reaction (COOR) was studied on steady-state conditions by chronoamperometry on polycrystalline smooth platinum and ruthenium rotating disc electrodes in CO-saturated acid solution. The chronoamperometric response did not show current oscillations and therefore the current density (j) vs. overpotential (η) curves on steady state could be obtained. In order to interpret these results, kinetic expressions were derived starting from the mechanism proposed by S. Gilman, which considers two adsorbed reaction intermediates, carbon monoxide (CO_{ad}) and hydroxyl (OH_{ad}). Analytical expressions as a function of overpotential for the current density, the surface coverage of the adsorbed species (θ_{CO} and θ_{OH}) and the CO and CO_2 pressures at the electrode surface on steady state were obtained. This set of equations was used for the correlation of the experimental polarization curves and the evaluation of the corresponding kinetic parameters. From these values, the dependences of the surface coverage of the adsorbed intermediates on overpotential were simulated, as well as those of the partial pressure of CO and CO_2. Thus, it was demonstrated that the Gilman's mechanism accurately describes the experimental results on steady state of the COOR on these metals.

Keywords CO electrooxidation · Kinetic mechanism · Platinum · Ruthenium

M. S. Rau · M. R. Gennero de Chialvo · A. C. Chialvo (✉)
Programa de Electroquímica Aplicada e Ingeniería Electroquímica (PRELINE), Facultad de Ingeniería Química,
Universidad Nacional del Litoral,
Santiago del Estero 2829,
3000 Santa Fe, Argentina
e-mail: achialvo@fiq.unl.edu.ar

Introduction

The electrochemical carbon monoxide oxidation reaction (COOR) is a process of technological as well as fundamental importance, and it serves as a model reaction in the electrocatalysis of small organic molecules [1]. Otherwise, the presence of carbon monoxide in the hydrogen feed is one of the fundamental problems related to practical application of low-temperature polymer electrolyte fuel cells, where the anode catalyst surface, usually Pt, is progressively blocked by adsorbed CO species leading to severe fuel cell performance losses [2]. This problem led to the search for CO-tolerant hydrogen oxidation catalysts [3]. In this sense, Pt–Ru alloys have emerged as the most promising candidates for the oxidation of CO [4]. In this context, the study of the COOR on both Pt and Ru electrodes remains an important subject, even more if it is taken into account that the available information about the kinetic parameters that characterizes the global reaction is scarce.

The methodology usually employed for the evaluation of the CO oxidation is the stripping voltammetry, where a monolayer of CO adsorbed at low potentials for different periods of time (1–60 min) is removed by a voltammetric sweep in absence of CO in solution. This method was applied on both supported and unsupported catalysts such as polycrystalline Pt [5–9], Pt single crystals [10–15], polycrystalline [16, 17], and single crystal Ru [18, 19], as well as Pt–Ru alloys [20]. Although there is a great deal of experimental information, as well as interpretation of the corresponding results, this type of experimental design does not allow the rigorous evaluation of the electrocatalytic activity of a given material for the COOR, as the electrocatalytic activity is related to the capacity of the material to improve the global reaction rate. The CO adsorption is

carried out in acid solution at a potential [0.05–0.2 V vs. reversible hydrogen electrode (RHE)] where oxidation does not take place. Moreover, the adsorption time is usually long enough to permit that CO_{ad} reaches the equilibrium condition, while the oxidation is verified at potentials significantly higher (E>0.5 V). These conditions do not correspond to the occurrence of the COOR, where simultaneously the CO adsorption, the water electrosorption and the electrochemical oxidation are taking place at a given potential.

Other type of measurements consisted in the application of potentiodynamic sweeps in the presence of CO in solution, including or not the preadsorption of CO at a constant potential [21–26]. In this sense, Gasteiger et al. [22] studied the electrooxidation of CO on rotating disk electrodes of Pt, Ru, and Pt–Ru on CO-saturated 0.5 M H_2SO_4 solution through voltammetric sweeps run at 20 mV s^{-1}. Then Gasteiger et al. [20] studied the bulk CO oxidation on a polycrystalline Pt electrode with a hydrodynamic wall-jet EQCN setup, being the electrode potential scan rate 10 mV s^{-1} and the electrolyte flow rate 1 ml s^{-1}. More recently, Zhang et al. [26] analyzed the interaction of mass transport and reaction kinetics during the CO oxidation on Pt in a thin-layer flow cell. They applied CO_{ad} stripping as well as bulk CO voltammetric oxidation, including the description of the mass transport processes. These types of measurements are characterized by the influence of the pseudocapacitive process originated in the variation of the CO surface coverage during the voltammetric scan. An interesting experiment that illustrate this behavior consisted in the comparison of the peak current density of the stripping (≅100 μA cm^{-2}) with the value obtained when the sweep is stopped at the peak potential during 3 min (23 μA cm^{-2}) [27]. The modelling of all the processes involved in the bulk CO voltammetric oxidation is extraordinarily complex and necessarily involve kinetic approximations [26].

Another aspect that should be mentioned is that experimental measurements carried out under galvanostatic conditions have shown an oscillation process in the potential response [28–30]. On the other hand, under potentiostatic conditions the existence of such instabilities is uncertain, but they were clearly observed in the presence of inhibiting anions, BF_4^- [31] or Cl^- [32]. A kinetic model was developed, involving the anion adsorption, to explain such behavior [31].

Furthermore, a kinetic model for the CO electrooxidation was developed recently with the aim of the determination of the apparent transfer coefficient through the use of a potential modulation technique [33]. However, there have been no reports concerning the correlation of experimental data of the COOR obtained in steady state from chronoamperometry and the calculation of the corresponding kinetic parameters. This type of measurement is characterized by the absence of pseudocapacitive processes, which are present when voltammetric scans are applied to study the COOR.

In this context, the present work deals with the resolution of the kinetic mechanism of the COOR on steady state, the derivation of the kinetic expressions and the correlation of experimental results obtained on polycrystalline Pt and Ru electrodes in sulphuric acid solution saturated with CO through potentiostatic measurements carried out under controlled mass transport conditions. The corresponding kinetic parameters will be also evaluated and the behavior of the adsorbed species will be simulated and discussed.

Experimental

The electrochemical COOR:

$$CO + H_2O \rightleftharpoons CO_2 + 2H^+ + 2e^- \quad (1)$$

was studied through the determination of the steady-state dependence $j(\eta)$. The experimental measurements were carried out in a three electrodes cell specially built for the use of a rotating electrode and with a particular design of the gas saturator. The working electrodes were rotating discs of polycrystalline platinum 99.99% (Radiometer) and ruthenium 99.95% (MaTecK) with a geometric area of 0.07 cm^2. The rotation rate was varied in the range 2,500 rpm≤ω≤8,100 rpm through the use of a rotating disk Radiometer EDI 10 K. The counterelectrode was a platinum helical wire of large area. The electrolytic solution was 0.5 M H_2SO_4, prepared with ultra-pure water (PureLab, Elga LabWater). Measurements were carried out at 25 °C under CO gas bubbling at 1 atm, ensuring a continuous saturation of the electrolyte. The applied overpotentials were controlled with respect to an RHE in the same solution. In order to calculate the value of the equilibrium potential (E^e) in Eq. 1 with respect to RHE in the working conditions, the following cell was considered: Pt, H_2(1 atm)/H_2SO_4(0.5 M)/CO(P_{CO}), CO_2 (P_{CO2}), Pt. Taking into account that the normal potential of the CO/CO_2 electrode is E^o_{CO/CO_2}=0.106 V [34] and that the CO used contains 30 ppm of CO_2, the value of the equilibrium potential of the CO oxidation reaction with respect to the RHE calculated by the Nernst equation was E^e=−0.025 V.

Before the experimental determinations corresponding to the COOR, the working electrode (Pt or Ru) was mechanically polished with emery paper 1,200 grit, followed by sonication in ultra-pure water for 5 min. The electrochemical characterization of the electrode surface was carried out by cyclic voltammetry at 0.1 Vs^{-1} in the electrolyte solution saturated with nitrogen gas in the range

0.0–1.5 V (Pt) and 0.0–0.9 V (Ru). In all cases, it was verified that the stabilized voltammogram had the appropriate potentiodynamic profile for the experimental conditions.

All the experimental determinations for the study of the COOR were carried out in the electrolyte solution saturated with carbon monoxide at a given rotation rate in the following overpotential ranges: 0.7 V≤η≤1.4 V for Pt and 0.2 V≤η≤0.8 V for Ru. The determination of the experimental current–overpotential dependences for the COOR on steady state was carried out through the application of a sequence of potentiostatic pulses of 0.1 V starting from 0.2 V (Ru) and 0.7 V (Pt). Each overpotential value was maintained during 3 min and during this period, the current value was measured each 0.1 s and the mean value of the last 10 s was assigned to this overpotential. Certain points, where it was observed that current was not constant enough, were repeated for a longer period of time. Additionally, potentiodynamic measurements were also carried out, consisting in voltammetric sweeps run at 0.01 Vs^{-1} in the same range of overpotentials than those used for the steady-state polarization curves.

Results

The first experiments carried out consisted in long-term chronoamperometric measurements (60 min) in order to analyse the existence of oscillation in the current response. It has not been observed in these experiments carried out at different overpotential values any oscillatory behavior. This issue was important in order to carry out the proposed kinetic study in steady state, which results are going to be described.

Figure 1 shows the experimental current density–overpotential dependences for the COOR in a polycrystalline smooth platinum electrode rotated at 4,900 rpm in a 0.5 M H_2SO_4 solution saturated with carbon monoxide (30 ppm CO_2) at P=1 atm. The continuous line corresponds to the potentiodynamic sweep run at 0.01 Vs^{-1}, while symbols are the response to the potentiostatic pulses. It can be observed that there is a large difference between them. The potentiodynamic profile exhibits the influence of pseudocapacitive effect as well as a pronounced hysteresis, with the presence of an anodic peak at 0.88 V in the cathodic sweep. It also showed a current increase with rotation rate. A similar voltammogram was previously obtained by other authors [22, 24, 25]. The steady-state curve shows, as it is expected, current values much smaller, with a well-defined peak located at approximately 0.97 V followed by a current plateau.

The corresponding results obtained for the COOR on the polycrystalline Ru electrode at 4,900 rpm are shown in Fig. 2. The potentiodynamic response (continuous line)

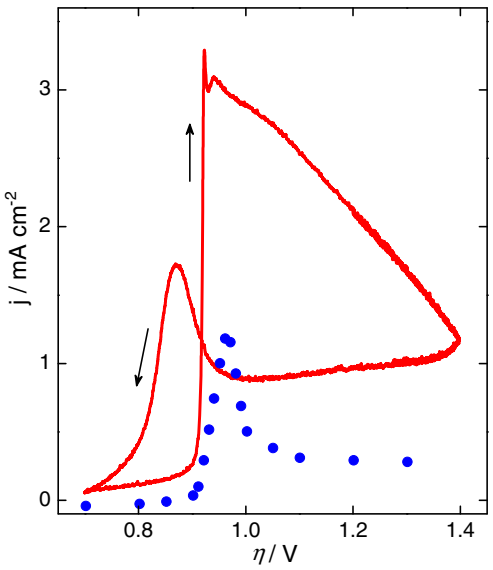

Fig. 1 Experimental $j(\eta)$ curves for the COOR on polycrystalline Pt in the range 0.7 V≤η≤1.4 V at ω=4,900 rpm. *Continuous line* Potentiodynamic sweep at 0.01 Vs^{-1}, *symbols* potentiostatic pulses, 0.5 M H_2SO_4, 25 °C

shows also pseudocapacitive effects and a double crossing between the anodic and cathodic sweeps, similar to the results obtained by Brankovic et al. [23]. The effect of the rotation rate is in this case almost negligible, although not null. The curve corresponding to the steady-state measurements (dots) shows a peak located at approximately 0.7 V. It should be noticed that the values of the current density obtained on ruthenium are much less than those delivered on platinum. On the other hand, the variation with the rotation rate of the experimental dependence $j(\eta)$ obtained

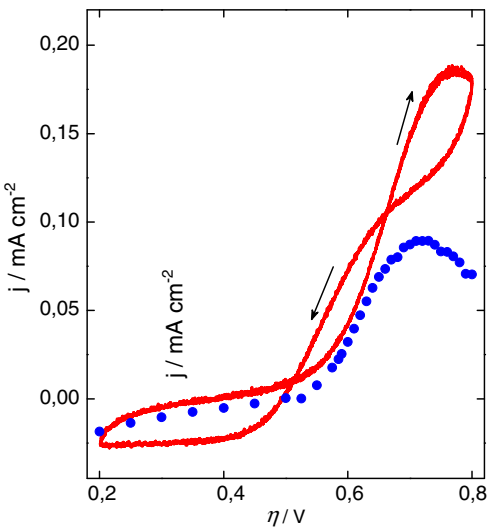

Fig. 2 Experimental $j(\eta)$ curves for the COOR on polycrystalline Ru in the range 0.2 V≤η≤0.8 V at ω=4,900 rpm. *Continuous line* Potentiodynamic sweep at 0.01 Vs^{-1}, *symbols* potentiostatic pulses, 0.5 M H_2SO_4, 25 °C

in potentiostatic conditions for the COOR is small for Pt and almost negligible for Ru, at least for ω>2,500 rpm. This behavior can be explained considering the Levich–Koutecky equation [35]. As the limiting diffusion current density of CO is greater than the current densities involved in the experimental determinations, especially for the Ru electrode, the influence of ω should be small.

In order to interpret the results obtained, it has been developed and solved a kinetic model, which includes the description of the surface coverage of the reaction intermediates as well as the variation of the CO gas pressure at the electrode surface on overpotential.

Kinetic description

The following three steps are considered for the kinetic mechanism of the COOR on a metallic surface, following that suggested by Gilman [36]:

$$\text{CO adsorption}: \quad \mathrm{CO + S \underset{v_{-1}}{\overset{v_{+1}}{\rightleftarrows}} CO_{ad}} \tag{2.1}$$

$$\mathrm{H_2O}\ \text{electrosorption}: \quad \mathrm{H_2O + S \underset{v_{-2}}{\overset{v_{+2}}{\rightleftarrows}} OH_{ad} + H^+ + e^-} \tag{2.2}$$

$$\text{CO oxidation}: \quad \mathrm{CO_{ad} + OH_{ad} \underset{v_{-3}}{\overset{v_{+3}}{\rightleftarrows}} CO_2 + H^+ + e^- + 2\,S} \tag{2.3}$$

where S represents a free active site on the electrode surface in which the reaction intermediates CO_{ad} and OH_{ad} can be adsorbed. v_{+i} and v_{-i} are the forward and backward reaction rate of the step i (i=1,2,3), respectively, being v_i=v_{+i}-v_{-i} the reaction rate of the step i. The free sites S could be occupied also by the adsorption of the anions of the electrolyte, SO_4=/HSO_4^-, but on the basis of experiments carried out in H_2SO_4 and $HClO_4$ (nonadsorbable anion) solutions, it can be considered that the influence of anions adsorption on Pt can be neglected (see Fig. 8 in Ref. [30]). Meanwhile, the strong interaction of OH with Ru also prevents the anions adsorption on this electrode [37]. Then the expressions of the reaction rates of the three steps involved in the kinetic mechanism can be written as:

$$v_1 = k_{+1}(1-\theta)P^{\mathrm{s}}_{\mathrm{CO}} - k_{-1}\theta_{\mathrm{CO}} \tag{3}$$

$$v_2 = k_{+2}a_{\mathrm{H_2O}}(1-\theta)\mathrm{e}^{\alpha_2 fE} - k_{-2}a_{\mathrm{H^+}}\theta_{\mathrm{OH}}\mathrm{e}^{(\alpha_2-1)fE} \tag{4}$$

$$v_3 = k_{+3}\theta_{\mathrm{CO}}\theta_{\mathrm{OH}}\mathrm{e}^{\alpha_3 fE} - k_{-3}a_{\mathrm{H^+}}P^{\mathrm{s}}_{\mathrm{CO_2}}(1-\theta)^2\mathrm{e}^{(\alpha_3-1)fE} \tag{5}$$

The surface coverage (θ) is the sum of two contributions, the carbon monoxide coverage (θ_{CO}) and the hydroxyl coverage (θ_{OH}) respectively:

$$\theta = \theta_{\mathrm{CO}} + \theta_{\mathrm{OH}} \tag{6}$$

Moreover, k_{+i} and k_{-i} are the forward and backward kinetic constants of the step i (i=1, 2, 3); P_i^s is the pressure of the gas i (i=CO, CO_2) at the electrode surface; a_i is the activity of the species i (i=H_2O, H^+); α_i is the symmetry factor of the step i (i=2, 3); E is the electrode potential and f=F/RT.

The corresponding expressions of the equilibrium reaction rates (v_i^e), compatible with the reversibility microscopic principle, are obtained through the application of the equilibrium condition (v_i=0) to Eqs. 3, 4 and 5:

$$v_1^{\mathrm{e}} = k_{+1}(1-\theta^{\mathrm{e}})P^{\mathrm{e}}_{\mathrm{CO}} = k_{-1}\theta^{\mathrm{e}}_{\mathrm{CO}} \tag{7}$$

$$v_2^{\mathrm{e}} = k_{+2}a_{\mathrm{H_2O}}(1-\theta^{\mathrm{e}})\,\mathrm{e}^{\alpha_2 fE^{\mathrm{e}}} = k_{-2}a_{\mathrm{H^+}}\theta^{\mathrm{e}}_{\mathrm{OH}}\mathrm{e}^{(\alpha_2-1)fE^{\mathrm{e}}} \tag{8}$$

$$v_3^{\mathrm{e}} = k_{+3}\theta^{\mathrm{e}}_{\mathrm{CO}}\theta^{\mathrm{e}}_{\mathrm{OH}}\mathrm{e}^{\alpha_3 fE^{\mathrm{e}}} = k_{-3}a_{\mathrm{H^+}}P^{\mathrm{e}}_{\mathrm{CO_2}}(1-\theta^{e})^2\mathrm{e}^{(\alpha_3-1)fE^{\mathrm{e}}} \tag{9}$$

where the superscript e indicates the equilibrium condition. Dividing each equation of v_i by the corresponding equation of v_i^e, the following expressions are obtained:

$$v_1 = v_1^{\mathrm{e}}\left[\frac{(1-\theta)P^{\mathrm{s}}_{\mathrm{CO}}}{(1-\theta^{\mathrm{e}})P^{\mathrm{e}}_{\mathrm{CO}}} - \frac{\theta_{\mathrm{CO}}}{\theta^{\mathrm{e}}_{\mathrm{CO}}}\right] \tag{10}$$

$$v_2 = v_2^{\mathrm{e}}\left[\frac{(1-\theta)\mathrm{e}^{\alpha_2 f\eta}}{1-\theta^{\mathrm{e}}} - \frac{\theta_{\mathrm{OH}}\mathrm{e}^{(\alpha_2-1)f\eta}}{\theta^{\mathrm{e}}_{\mathrm{OH}}}\right] \tag{11}$$

$$v_3 = v_3^{\mathrm{e}}\left[\frac{\theta_{\mathrm{OH}}\theta_{\mathrm{CO}}\mathrm{e}^{\alpha_3 f\eta}}{\theta^{\mathrm{e}}_{\mathrm{OH}}\theta^{\mathrm{e}}_{\mathrm{CO}}} - \frac{(1-\theta)^2P^{\mathrm{s}}_{\mathrm{CO_2}}\mathrm{e}^{(\alpha_3-1)f\eta}}{(1-\theta^{\mathrm{e}})^2P^{\mathrm{e}}_{\mathrm{CO_2}}}\right] \tag{12}$$

where η is the overpotential (η=E-E^e) for the COOR.

The step of H_2O electrosorption can be considered in equilibrium at each overpotential [38], which implies that $v_2/v_2^e \to 0$. Consequently, under this approximation, the bracket in Eq. 11 is null, and therefore, the relationship between the surface coverage of OH_{ad} and that of the CO_{ad} can be obtained:

$$\frac{\theta_{\mathrm{OH}}}{\theta^{\mathrm{e}}_{\mathrm{OH}}} = \frac{(1-\theta_{\mathrm{CO}})\mathrm{e}^{f\eta}}{1-\theta^{\mathrm{e}}+\theta^{\mathrm{e}}_{\mathrm{OH}}\mathrm{e}^{f\eta}} \tag{13}$$

Moreover, the relationship between the concentration of the free sites (1–θ) and that of the CO_{ad} is obtained from Eqs. (6) and (13):

$$\frac{1-\theta}{1-\theta^{e}} = \frac{1-\theta_{CO}}{1-\theta^{e}+\theta^{e}_{OH}e^{f\eta}} \tag{14}$$

Furthermore, it is necessary to know the relationship between the gas pressure at the electrode surface and that on the bulk (P_i^s/P_i^e, i=CO, CO_2), which can be related to the corresponding relationship between the current density at a given overpotential and the limiting diffusion current density [$j(\eta)/j_L^i$, i=CO, CO_2]:

$$\frac{P^{s}_{CO}}{P^{e}_{CO}} = 1 - \frac{j(\eta)}{j_L^{CO}} \tag{15}$$

$$\frac{P^{s}_{CO_2}}{P^{e}_{CO_2}} = 1 + \frac{j(\eta)}{\left|j_L^{CO_2}\right|} \tag{16}$$

Finally, taking into account that the reaction rate of the overall reaction (V) can be related to those of the steps (V=v_1=v_3) and that j=2FV, two expressions of the dependence $j(\eta)$ can be obtained. One of them becomes from the substitution of Eq. 15 into Eq. 10 and rearranging:

$$j = \left[\frac{1-\theta}{1-\theta^{e}} - \frac{\theta_{CO}}{\theta^{e}_{CO}}\right]\left[\frac{1}{2Fv_1^{e}} + \frac{1-\theta}{j_L^{CO}(1-\theta^{e})}\right]^{-1} \tag{17}$$

The other is obtained by substitution of Eq. (16) into Eq. (12) and reordering:

$$j = \left[\frac{\theta_{CO}\theta_{OH}e^{\alpha_3 f\eta}}{\theta^{e}_{CO}\theta^{e}_{OH}} - \frac{(1-\theta)^2 e^{(\alpha_3-1)f\eta}}{(1-\theta^{e})^2}\right]\left[\frac{1}{2Fv_3^{e}} + \frac{(1-\theta)^2 e^{(\alpha_3-1)f\eta}}{\left|j_L^{CO_2}\right|(1-\theta^{e})^2}\right]^{-1} \tag{18}$$

Substituting Eqs. 13 and 14 into Eqs. 17 and 18 and equalizing them, the following implicit equation of the dependence $\theta_{CO}(\eta)$ is obtained:

$$\left[\frac{1-\theta_{CO}}{1-\theta^{e}+\theta^{e}_{OH}e^{f\eta}} - \frac{\theta_{CO}}{\theta^{e}_{CO}}\right]\left[\frac{1}{2Fv_3^{e}} + \frac{(1-\theta_{CO})^2 e^{(\alpha_3-1)f\eta}}{\left|j_L^{CO_2}\right|\left(1-\theta^{e}+\theta^{e}_{OH}e^{f\eta}\right)^2}\right] - \left[\frac{\theta_{CO}(1-\theta_{CO})e^{(1+\alpha_3)f\eta}}{\theta^{e}_{CO}\left(1-\theta^{e}+\theta^{e}_{OH}e^{f\eta}\right)} - \frac{(1-\theta_{CO})^2 e^{(\alpha_3-1)f\eta}}{\left(1-\theta^{e}+\theta^{e}_{OH}e^{f\eta}\right)^2}\right]\left[\frac{1}{2Fv_1^{e}} + \frac{(1-\theta_{CO})}{j_L^{CO}\left(1-\theta^{e}+\theta^{e}_{OH}e^{f\eta}\right)}\right] = 0 \tag{19}$$

Therefore, using the Eq. (17) or (18), Eq. (13) and Eq. (19), the experimental dependence $j(\eta)$ obtained in steady-state conditions for the COOR on a given metal electrode can be correlated and the values of the equilibrium reaction rates of the CO adsorption step (v_1^e) and of the electrooxidation step (v_3^e), the equilibrium surface coverage of OH_{ad} (θ^e_{OH}) and CO_{ad} (θ^e_{CO}) and the symmetry factor of the electrooxidation step (α_3) can be evaluated, if the values of the limiting diffusion current density of CO (j_L^{CO}) and CO_2 ($j_L^{CO_2}$) are known.

Evaluation of the kinetic parameters

The experimental dependences $j(\eta)$ obtained in steady-state conditions for the COOR were correlated with the expressions derived from the resolution of the proposed kinetic mechanism. The corresponding values for the limiting diffusion current densities of carbon monoxide (j_L^{CO}) and carbon dioxide ($j_L^{CO_2}$) in the electrolyte solution were calculated by the use of the Levich equation $j_L = B\omega^{1/2}$ [39]. Constant B was accurately measured for hydrogen gas in 0.5 M H_2SO_4 solution and similar operating conditions [40]. Therefore, the constant B values for CO and CO_2 were evaluated through the correction of the corresponding value for H_2, taking into account that:

$$B_i = \left(\frac{D_i}{D_{H_2}}\right)^{2/3}\left(\frac{C_i^{o}}{C_{H_2}^{o}}\right)B_{H_2} \quad ; \quad i = CO, CO_2 \tag{20}$$

where D_i is the diffusion coefficient and C_i^o is the solubility of the gas i in the electrolyte solution. The values of the parameters needed for the evaluation as well as the resulting values of the constant B are illustrated in Table 1 [40–42].

The correlation of the dependences $j(\eta)$ obtained at steady state was carried out with Eq. 17 or 18 and Eq. 19 and taking into account Eqs. 6 and 13. The varied kinetic parameters in the correlation were v_1^e, v_3^e, θ^e_{OH}, θ^e_{CO}, and α_3. The calculations were made by nonlinear least squares regression, using the software Micromath Scientist 2.0, in the overpotentials range 0.83 V≤η≤1.02 V for Pt and 0.47 V≤η≤0.82 V for Ru. The range corresponds in each case to the higher current values. For more anodic overpotentials, the oxidation reaction takes place on a surface covered by a metal oxide layer, where the kinetic mechanism may not be applicable.

The resulting values of the parameters are shown in Table 2 for Pt and Ru electrodes. The values of the

Table 1 Values of the diffusion coefficient (D) [41], the solubility (C^o) [42] and the Levich constant (B) of H_2 [40], CO, and CO_2 in water at 25 °C

Gas	D 10^5 (cm^2 s^{-1})	C^o 10^4 (mol dm^{-3})	B 10^5 (A cm^{-2} rpm$^{-1/2}$)
H_2	4.50	7.84	6.88
CO	2.03	9.86	5.09
CO_2	1.92	342.0	170.1

Table 2 Kinetic parameters of the COOR on Pt and Ru electrodes obtained from the correlation of the experimental $j(\eta)$ curves in steady state

Kinetic parameter	Pt	Ru
v_1^e (mol cm^{-2} s^{-1})	7.89×10^{-9}	3.62×10^{-10}
v_3^e (mol cm^{-2} s^{-1})	1.44×10^{-31}	1.57×10^{-22}
θ^e_{CO}	0.6445	0.251
θ^e_{OH}	1.95×10^{-17}	1.05×10^{-14}
α_3	0.428	0.191

equilibrium reaction rate of the CO adsorption step v_1^e for Pt and Ru are rather similar. Meanwhile, the equilibrium reaction rate of the electrooxidation step v_3^e is in both cases much less than v_1^e, being $v_3^e(\text{Ru})>v_3^e(\text{Pt})$. This difference is due to that, on ruthenium, the COOR starts at an overpotential approximately 0.35 V less than that of platinum. However, it should be noticed that the beginning of the reaction needs significantly high overpotential values (η>0.5 V for Ru and η>0.9 V for Pt). It is likely that CO itself acts as an inhibitor of the COOR, as it is highly adsorbed on the metallic surface, meanwhile, the coverage of OH_{ad} is almost negligible. It should be noticed that the value obtained for Pt (θ^e_{CO}=0.64) is near the saturation coverage (θ_{CO}=0.68) found for Pt(111) [43]. The corresponding value for ruthenium was $\theta^e_{CO}\cong0.25$, indicating a lower CO adsorption capability than platinum.

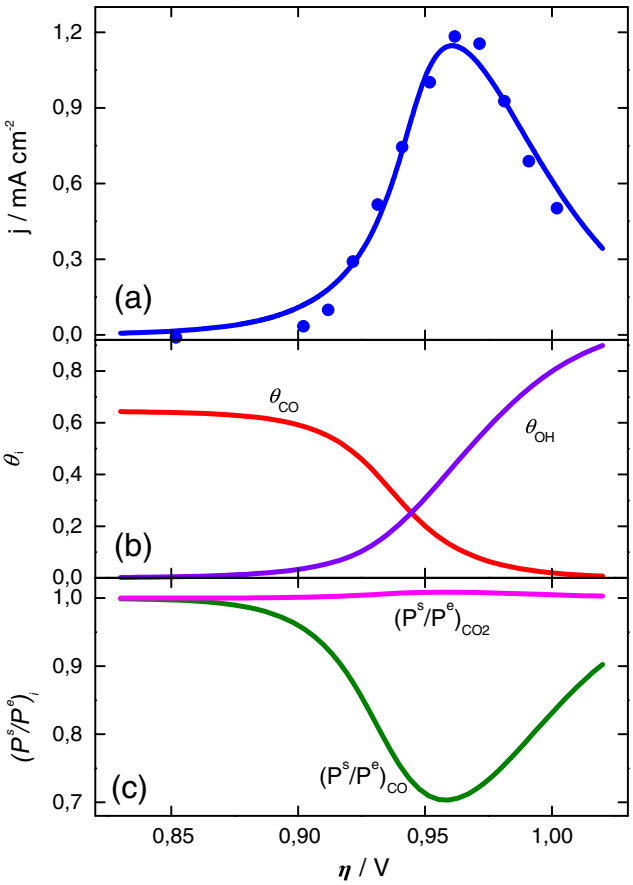

Fig. 3 **a** Experimental (*symbols*) and simulated (*lines*) $j(\eta)$ curves of the COOR on Pt in the range 0.83 V≤η≤1.02 V at ω=4,900 rpm. **b** Simulated dependences of $\theta_{CO}(\eta)$ and $\theta_{OH}(\eta)$. **c** Simulated dependences of $P^s_{CO}(\eta)/P^e_{CO}$ and $P^s_{CO_2}(\eta)/P^e_{CO_2}$. Kinetic parameters from Table 2

Discussion

From the resolution of the kinetic mechanism originally proposed by Gilman [36], commonly accepted for the CO electrooxidation reaction, theoretical expressions for the dependences $j(\eta)$, $\theta_{CO}(\eta)$, and $\theta_{OH}(\eta)$ were derived for the first time. Furthermore, starting from the experimental measurement of the dependence $j(\eta)$ through the use of a rotating disc electrode of polycrystalline Pt and Ru in acid solution saturated with CO, having previously verified the absence of current oscillation, the kinetic parameters of the COOR could be determined on both metals.

The polarization curves corresponding to Pt (Fig. 1, dots) and Ru (Fig. 2, dots) were simulated using the kinetic parameters of Table 2. They are shown in Fig. 3a (Pt) and Fig. 4a (Ru) as continuous lines, where the experimental points are also included. It can be observed that the agreement between the experimental and fitted curves is good, demonstrating that the kinetic mechanism employed is appropriate to describe the COOR on these metal electrodes.

It should be noticed that the dependences $j(\eta)$ on steady state present a maximum value. This behavior is only possible if, as η increases, $\theta_{CO}(\eta)$ decreases while $\theta_{OH}(\eta)$ increases. Therefore, both dependences were simulated with the kinetic parameters given in Table 2. $\theta_{CO}(\eta)$ was evaluated from Eq. 19 and then $\theta_{OH}(\eta)$ was calculated from Eq. 13. The corresponding curves, shown in Fig. 3b (Pt) and Fig. 4b (Ru) respectively, are consistent with the predicted behavior. Moreover, as the water electroadsorption was considered at equilibrium, the $\theta_{OH}(\eta)$ dependence for the overpotentials where $\theta_{CO}\rightarrow0$ should be comparable to that obtained in a CO free solution. In this sense, Fig. 3b resembles that obtained by Imai et al. (Fig. 1 in Ref. [44]). The values of θ^e_{OH} indicate that at equilibrium conditions the adsorption of OH is almost negligible, which is in agreement with the usual consideration of null coverage in approximated kinetic analysis. In the present case such approximation would lead to a mathematical indeterminacy and therefore by correlation could be never obtained, but it can be considered null from a practical point of view. Moreover, it is in agreement with previous results found in the study of the influence of this species in the kinetics of the hydrogen oxidation reaction on ruthenium [45].

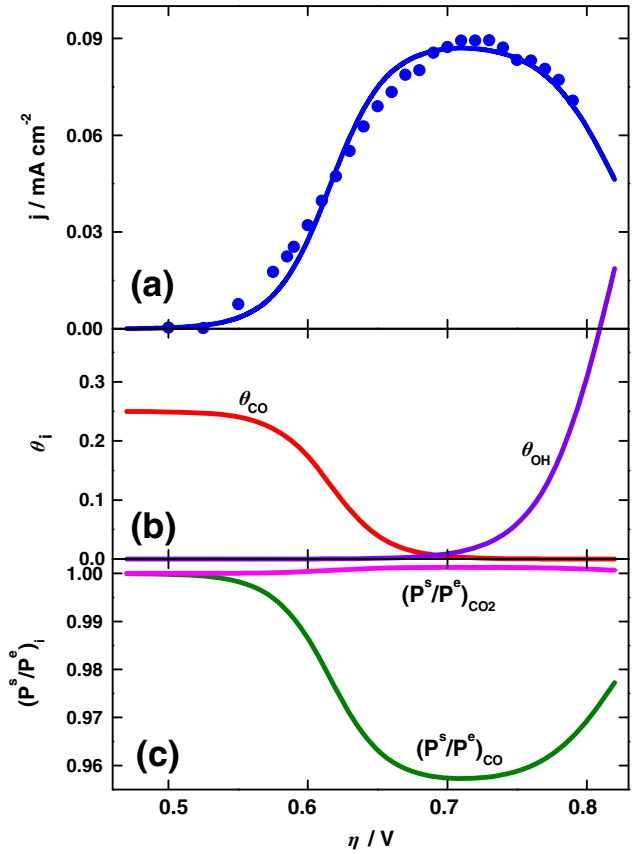

Fig. 4 **a** Experimental (*symbols*) and simulated (*lines*) $j(\eta)$ curves of the COOR on Ru in the range $0.47 \leq \eta \leq 0.82$ Vat ω = 4,900 rpm. **b** Simulated dependences of $\theta_{CO}(\eta)$ and $\theta_{OH}(\eta)$. c Simulated dependences of $P^{s}_{CO}(\eta)/P^{e}_{CO}$ and $P^{s}_{CO_2}(\eta)/P^{e}_{CO_2}$. Kinetic parameters from Table 2

However, the presence of CO_{ad} induces a lower value of $\theta^{e}_{OH}$with respect to the value obtained for the H_2 oxidation. Then, as the overpotential takes more anodic values, the increase in the surface coverage of OH_{ad} produces the increase of the reaction rate of the COOR. Nevertheless, the continuous growth of $\theta_{OH}(\eta)$ finally causes the continuous decrease of the CO adsorption, as this is a potential independent process, and therefore the reaction rate of the COOR also decreases. Therefore, it can be concluded that the main difference between Ru and Pt is the range of overpotentials where the reaction takes place, due to their different CO adsorption capability. This is consistent with the lower value of the equilibrium surface coverage θ^{e}_{CO} on Ru, as it implies a weaker adsorption.

It was also simulated for carbon monoxide and carbon dioxide respectively the relationship between the gas pressure on the reaction plane and in the bulk. $P^{s}_{CO}(\eta)/P^{e}_{CO}$ was calculated from Eq. (15) and $P^{s}_{CO_2}(\eta)/P^{e}_{CO_2}$ from Eq. (16). These curves are shown in Fig. 3c (Pt) and Fig. 4c (Ru). The relationship $P^{s}_{CO}(\eta)/P^{e}_{CO}$ passes through a minimum value at an overpotential which is coincident with the maximum current density. Otherwise, the relationship $P^{s}_{CO_2}(\eta)/P^{e}_{CO_2}$ presents a maximum at such current density although the variation is very low.

It should be noticed the marked difference between the experimental current–potential curves corresponding to the potentiodynamic sweep and the steady state, respectively. In the first case it can be clearly observed that the pseudocapacitive contribution is significantly greater than the faradaic current of the COOR for both electrodes. Consequently, the potentiodynamic experiments are not appropriate to evaluate the electrocatalytic activity.

Another aspect that can be analysed is the influence of the rotation rate on the potentiodynamic profile. It was already mentioned that there is an important effect of rotation rate in the case of Pt while in Ru the influence of ω is low, but not null. This behavior can be understood taking into account the difference between the value of the limiting diffusion current density of carbon monoxide (j^{CO}_{L}) and that of the maximum current density during the voltammetric CO oxidation. The value of j^{CO}_{L} at 4900 rpm calculated from Table 1 is 3.56 mA cm^{-2}, while the maximum is at approximately 3.0 mA cm^{-2} (Fig. 1, continuous line) for Pt and only 0.18 mA cm^{-2} (Fig. 2, continuous line) for Ru. Taking into account the Levich–Koutecky equation, the difference between this last value and j^{CO}_{L}can explain the small effect of ω for this metal. Then, the comparison of the maximum current densities corresponding to the steady-state measurements (Figs. 1 and 2, symbols) with j^{CO}_{L}indicates that the influence of the rotation rate should be very low for Pt and almost negligible for Ru.

Finally, on platinum it can be observed in the cathodic scan of the potentiodynamic sweep an anodic current approximately constant in the range comprised between 1.4 and 1.0 V. The steady-state curve shows a similar behavior in this overpotential range, but with less values of the current density. This result would indicate that, as OH_{ad} is transformed into PtO [44], this can participate in the reaction kinetics and thus the COOR at high overpotentials would be verified through a different mechanism than that used here. This process would need a more specific study.

Conclusions

The kinetic mechanism originally proposed by Gilman for the CO electrooxidation reaction was used to obtain the theoretical expressions for the dependences $j(\eta)$, $\theta_{CO}(\eta)$, $\theta_{OH}(\eta)$,$P^{s}_{CO}(\eta)/P^{e}_{CO}$, and $P^{s}_{CO_2}(\eta)/P^{e}_{CO_2}$ on steady state. Furthermore, the dependence $j(\eta)$ was experimentally obtained for polycrystalline platinum and ruthenium through chronoamperometric measurements carried out on rotating disc electrodes in acid solution saturated with CO, having previously verified the absence of current oscillation.

The correlation of these experimental curves with the set of equations derived, through the application of nonlinear least squares regression, established that the kinetic mechanism can reasonably describe the experimental results. Finally, the kinetic parameters of the COOR for both metals could be determined.

Acknowledgments The authors wish to acknowledge the financial support received from Agencia Nacional de Promoción Científica y Tecnológica, Consejo Nacional de Investigaciones Científicas y Técnicas and Universidad Nacional del Litoral.

References

1. Markovic NM, Ross PN Jr (2002) Surf Sci Rep 45:117–229
2. Lemons RA (1990) J Power Sources 29:251–264
3. Arico AS, Bruce P, Scrosati B, Tarascon J, Van Schalkwijk W (2005) Nat Mater 4:366–377
4. Maillard F, Lu GQ, Wieckowski A, Stimming U (2005) J Phys Chem B 109:16230–16243
5. Czerwinski A, Sobkowski A (1978) J Electroanal Chem 91:47–53
6. Couto A, Perez MC, Rincon A, Gutierrez C (1996) J Phys Chem 100:19538–19544
7. Hachkar M, Napporn T, Léger JM, Beden B, Lamy C (1996) Electrochim Acta 41:2721–2730
8. Kucernak AR, Offer GJ (2008) Phys Chem Chem Phys 10:3699–3711
9. Bergelin M, Wasberg M (1998) J Electroanal Chem 449:181–191
10. Herrero E, Feliu JM, Blais S, Radovic-Hrapovic Z, Jerkiewicz G (2000) Langmuir 11:4779–4783
11. Lin WF, Zei MS, Ertl G (1999) Chem Phys Lett 312:1–6
12. Gisbert R, García G, Koper MTM (2011) Electrochim Acta 56:2443–2449
13. Markovic NM, Grgur BN, Lucas CA, Ross PN (1999) J Phys Chem B 103:487–495
14. Bergelin M, Herrero E, Feliu JM, Wasberg M (1999) J Electroanal Chem 467:74–84
15. Batista EA, Iwasita T, Vielstich W (2004) J Phys Chem B 108:14216–14222
16. Zheng MS, Sun SG (2001) J Electroanal Chem 500:223–232
17. Gutierrez C, Caram JA, Beden B (1991) J Electroanal Chem 305:289–299
18. Lin WF, Christensen PA, Hamnett A, Zei MS, Ertl G (2000) J Phys Chem B 104:6642–6652
19. Wang WB, Zei S, Ertl G (2001) Phys Chem Chem Phys 3:3307–3311
20. Gasteiger HA, Markovic NM, Ross PN Jr, Cairns EJ (1994) J Phys Chem 98:617–625
21. Bavio MA, Kessler T, Castro Luna AM (2010) Int J Hydrogen Energy 35:5930–5933
22. Gasteiger HA, Markovic NM, Ross PN Jr (1995) J Phys Chem 99:8290–8301
23. Brankovic SR, Marinkovic NS, Wang JX, Adzic RR (2002) J Electroanal Chem 532:57–66
24. Ruvinskiy PS, Bonnefont A, Bayati M, Savinova ER (2010) Phys Chem Chem Phys 12:15207–15216
25. Stalnionis G, Tamasauskaite-Tamasiunaite L, Pautieniene V, Jusys Z (2006) J Electroanal Chem 590:198–206
26. Zhang D, Deutschmann O, Seidel YE, Behm RJ (2011) J Phys Chem C 115:468–478
27. Gutierrez C, Caram JA (1991) J Electroanal Chem 308:321–325
28. Deibert MC, Williams DL (1969) J Electrochem Soc 116:1290–1292
29. Morschl R, Bolten J, Bonnefont A, Krischer K (2008) J Phys Chem C 112:9548–9551
30. Koper MTM, Schmidt TJ, Markovic NM, Ross PN (2001) J Phys Chem B 105:8381–8386
31. Malkhandi S, Bonnefont A, Krischer K (2005) Electrochem Commun 7:710–716
32. Malkhandi S, Bonnefont A, Krischer K (2009) Surf Sci 603:1646–1651
33. Wang HC, Ernst S, Baltruschat H (2010) Phys Chem Chem Phys 12:2190–2197
34. Bard AJ, Parsons R, Jordan J (eds) (1985) Standard potentials in aqueous solutions. Marcel Dekker, New York
35. Bard AJ, Faulkner LR (2001) Electrochemical methods: fundamentals and applications. Wiley, Hoboken
36. Gilman S (1964) J Phys Chem 68:70–80
37. Marinkovic NS, Wang JX, Zajonz H, Adzic RR (2001) J Electroanal Chem 500:388–394
38. Koper MTM, Jansen APJ, van Santen RA, Lukkien JJ, Hilbers PAJ (1998) J Chem Phys 109:6051–6062
39. Gileadi E (1993) Electrode kinetics for chemistry, chemical engineering and material sciences. Wiley-VCH, Weinheim
40. Quaino PM, Gennero de Chialvo MR, Chialvo AC (2004) Phys Chem Chem Phys 6:4450–4455
41. Sherwood TK, Pigford RL, Wilke CR (1975) Mass transfer. Mc Graw-Hill, New York
42. Scharlin P, Battino R, Silla E, Tuñon I, Pascual-Ahuir JL (1998) Pure Appl Chem 70:1895–1904
43. Offer GJ, Kucernak AR (2008) J Electroanal Chem 613:171–185
44. Imai H, Izumi K, Matsumoto M, Kubo Y, Kato K, Imai Y (2009) J Am Chem Soc 131:6293–6300
45. Rau MS, Gennero de Chialvo MR, Chialvo AC (2010) Electrochim Acta 55:5014–5018